

# Strain-Induced Interlayer Magnetic Coupling Spike of the Two-Dimensional van der Waals Material $\text{Fe}_5\text{GeTe}_2$

Wen-Qiang Xie, Chang-Chun He, Xiao-Bao Yang, Yu-Jun Zhao,\* and Wen-Tong Geng\*

Cite This: *J. Phys. Chem. C* 2023, 127, 17194–17200

Read Online

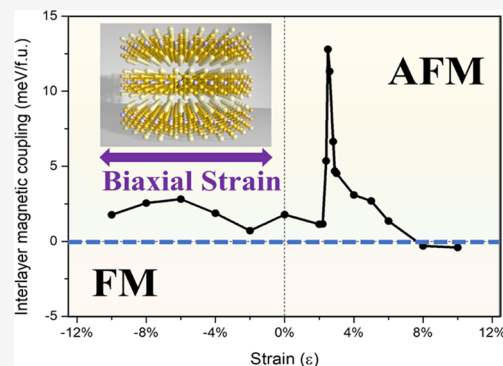
ACCESS |

Metrics & More

Article Recommendations

Supporting Information

**ABSTRACT:** A stronger interlayer magnetic coupling (ILMC) can open up new opportunities in spintronic devices. Numerous publications have demonstrated that ILMC is continuously evolving, even in the context of magnetic phase change. Here, we observe an extraordinary discontinuous transition (ILMC spike) in a two-dimensional (2D) van der Waals (vdW) material,  $\text{Fe}_5\text{GeTe}_2$  (F5GT). The ILMC spikes from 1.15 to 12.79 meV/f.u. when a 3% in-plane biaxial strain is applied. Additionally, the applied in-plane strain significantly enhances the magnetic anisotropy energy (MAE) of the system, triggering a sharp transition between the in-/off-plane configurations in multilayer F5GT.



## 1. INTRODUCTION

Magnetism in two-dimensional (2D) van der Waals (vdW) materials has attracted enormous attention in technological advances as its potential application ranges from topological magnonics to low-power spintronics and quantum computing.<sup>1–6</sup> Among the families of 2D vdW materials,  $\text{Fe}_5\text{GeTe}_2$  (F5GT) is a newly synthesized and promising vdW ferromagnet for spintronic devices due to its high Curie temperature (about 293 K)<sup>7</sup> and novel spintronic properties.<sup>8,9</sup> Strain engineering is an exciting and feasible method to manipulate the properties of materials in both theoretical and experimental investigations, which creates various opportunities for the study of new fundamental physics and applications of 2D vdW materials.<sup>10–13</sup> Meanwhile, 2D vdW materials were often transferred or grown onto a substrate such that the strain can be introduced by the substrate.<sup>10</sup> It has been observed that the magnetic properties of vdW materials are sensitive to the applied strain.<sup>14–17</sup>

A theoretical investigation of the strained single-layer F5GT has been reported.<sup>18</sup> However, spintronic devices are mainly based on multilayer vdW materials or heterostructures, such as giant magnetoresistance (GMR) and tunneling magnetoresistance (TMR)<sup>3–6</sup> devices. The presence of interlayer coupling could dramatically change the performance of devices.<sup>19,20</sup> Interlayer coupling can be divided into two parts, i.e., interlayer chemical coupling (ILCC) and interlayer magnetic coupling (ILMC),<sup>21</sup> which is of significance in terms of multilayer spintronics.<sup>9,22</sup> Numerous publications have demonstrated the continuous evolution of ILMC,<sup>23</sup> even in the context of magnetic phase change.<sup>24,25</sup> The discontinuous

transition feature in ILMC could encourage new avenues of research in spintronic devices.

In this work, we report a discontinuous transition feature (an impressive ILMC spike) induced by an in-plane strain in vdW F5GT. This extraordinary effect has significant implications for the design and performance of spintronic devices. In addition, we provide insights into the mechanism behind this ILMC spike through electronic structure analysis.

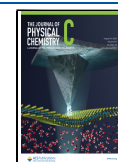
## 2. CALCULATIONS AND METHODS

The calculations were conducted based on the density functional theory,<sup>26,27</sup> by using the Vienna *ab initio* simulation package (VASP) code.<sup>28</sup> The projector augmented-wave (PAW)<sup>29</sup> method was employed with the Perdew–Burke–Ernzerhof (PBE)-type generalized gradient approximation (GGA) for describing the exchange–correlation potential.<sup>30</sup> As described in our previous study,<sup>8</sup> the lattice parameters calculated by PBE and LDA + U functionals are well in line with the measured values,<sup>31</sup> and the deviations are only  $-0.07$  Å (PBE) and  $0.03$  Å (LDA + U), respectively. The PBE functional underestimates the magnetic moments by the  $0.32 \mu_{\text{B}}/\text{Fe}$  ion; by comparison, the LDA + U functional overestimates by the  $1.04 \mu_{\text{B}}/\text{Fe}$  ion. Here, we choose the PBE functional for further calculations. Notably, the PBE

Received: June 5, 2023

Revised: July 25, 2023

Published: August 18, 2023



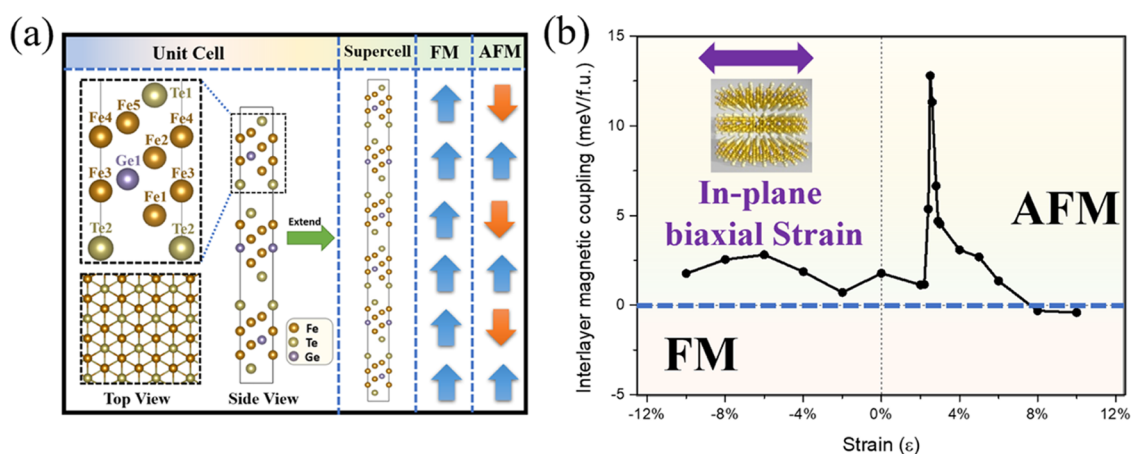


**Figure 1.** (a) Illustrative structure of  $\text{Fe}_5\text{GeTe}_2$  and the magnetic configurations of interlayer FM/AFM states. (b) Interlayer magnetic coupling (ILMC) evolution with in-plane biaxial strain.

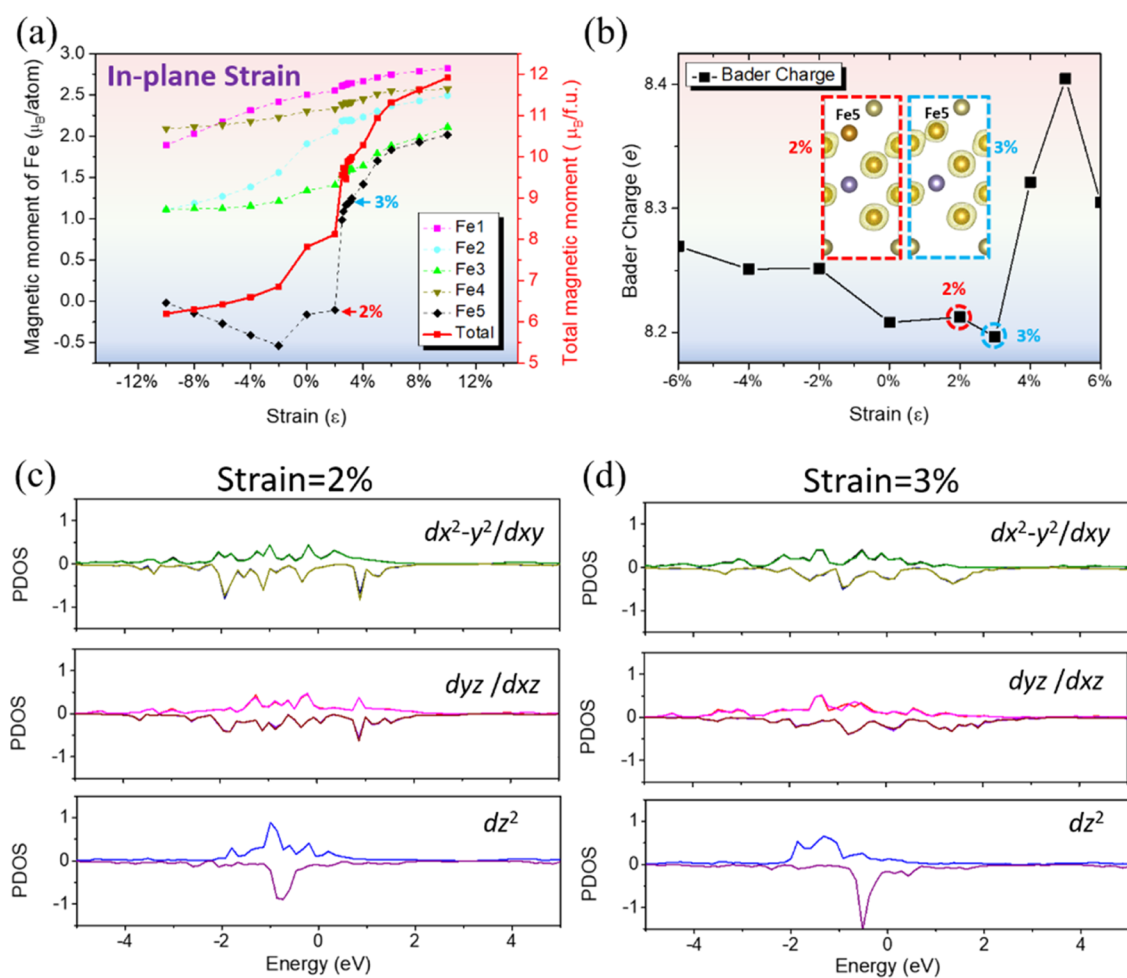


**Figure 2.** (a) Variation in the magnetic moments of Fe ions caused by the in-plane strain. (b) Bader charge variation of the Fe5 ion with in-plane strains. Inset: spin density with 2 and 3% in-plane strains. Projected density of states (PDOS) of the Fe5 ion under (c) a 2% and (d) a 3% in-plane strain.

calculated energy of the AFM configuration is lower than the FM configuration by 1.45 meV per formula unit (meV/f.u.), implying that F5GT prefers an AFM coupling. Similar results were also discussed in the  $\text{Fe}_3\text{GeTe}_2$  system.<sup>32</sup> A cutoff energy of 560 eV for the plane-wave basis set was applied to ensure an energy convergence of  $10^{-6}$  eV for the electronic structure. The reciprocal space integrations were sampled with a  $k$ -mesh

of  $10 \times 10 \times 1$  obtained by the  $\Gamma$ -centered Monkhorst–Pack method.<sup>33</sup> For the PBE functional, the vdW effect was considered by the DFT-D3 method with the Becke–Johnson potential.<sup>34</sup> The interlayer magnetic coupling (ILMC) and the interlayer chemical coupling (ILCC) are defined as follows

$$\text{ILMC} = E_{\text{FM}} - E_{\text{AFM}} \quad (1)$$

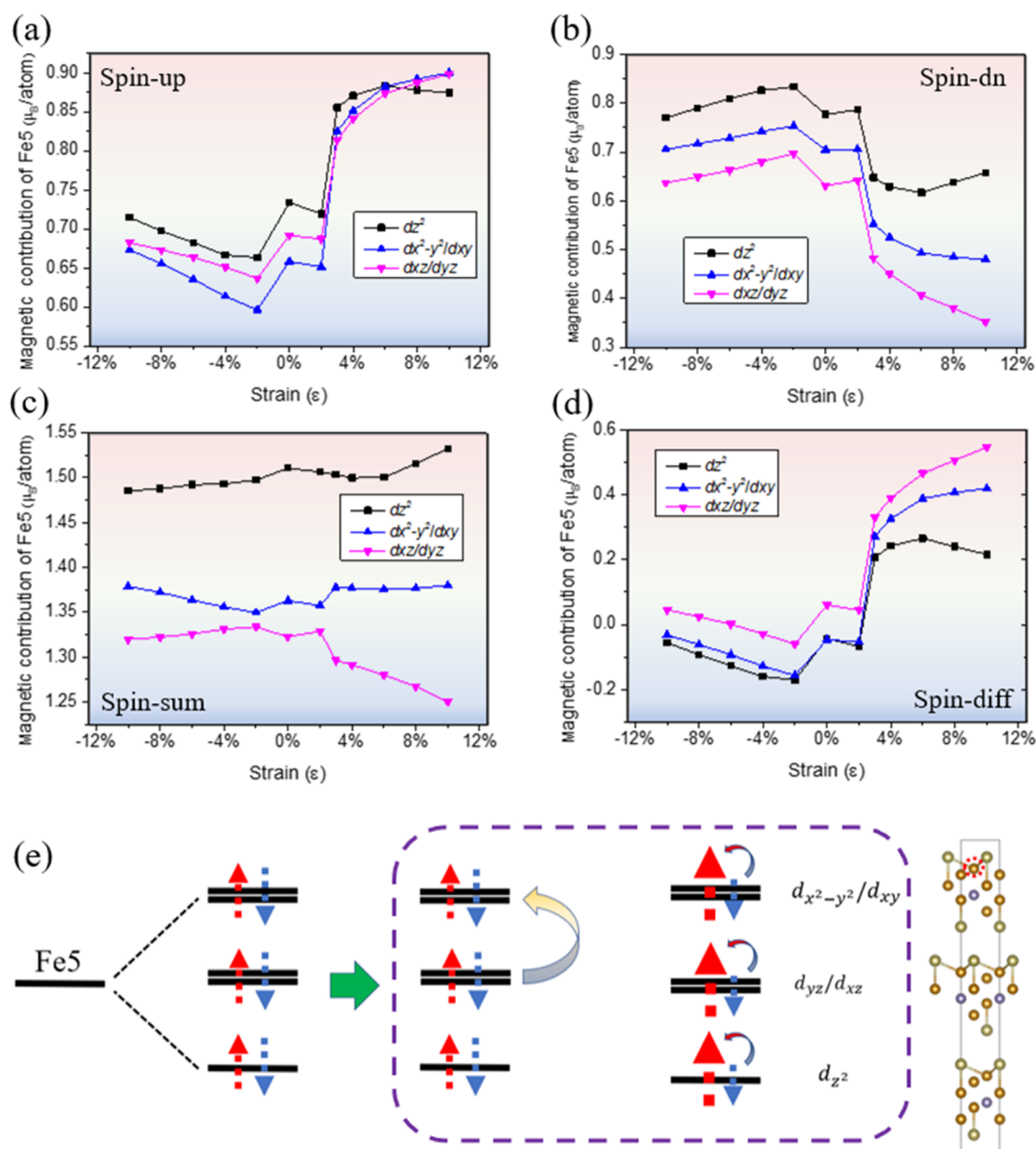


**Figure 3.** Mulliken population analysis of the Fe5 ion: (a) decomposed spin-up and (b) spin-down channels. (c) Sum of spin-up and spin-down channels. (d) Difference between spin-up and spin-down channels. (e) Proposed mechanism of the acute increase of the Fe5 magnetic moment.

$$ILCC = E_{\text{multi-layer}} - E_{\text{single-layer}} \quad (2)$$

Here,  $E_{\text{AFM}}$  is the energy of antiferromagnetic (AFM)  $\text{Fe}_5\text{GeTe}_2$  (FSGT) and  $E_{\text{FM}}$  is for the ferromagnetic (FM) FSGT.  $E_{\text{multi-layer}}$  and  $E_{\text{single-layer}}$  indicate the energies of multilayer (bulk and double layers) and single-layer FSGT, respectively. Magnetic anisotropy energy (MAE) is defined as

$$MAE = E_{\text{in-plane}} - E_{\text{off-plane}} \quad (3)$$

Here,  $E_{\text{in-plane}}$  stands for the energy with in-plane magnetization (parallel to the FSGT plane), while  $E_{\text{off-plane}}$  represents the off-plane magnetization (perpendicular to the FSGT plane). To ensure the accuracy of MAE, the  $k$ -mesh was set to  $12 \times 12 \times 1$ . The MAE changes within 0.04 meV when the  $k$ -mesh increases from  $12 \times 12 \times 1$  to  $16 \times 16 \times 1$ . The exchange parameters for the Heisenberg model are calculated depending on the localized basis functions.<sup>35</sup> VASP is based on a plane-

wave basis, while OpenMX is based on pseudo-atomic localized basis functions.<sup>36</sup> Therefore, the Heisenberg exchange parameters were studied using OpenMX<sup>36</sup> and a postprocessing code based on Green's function.<sup>37</sup> We conducted the related calculation using the PBE functional, with a  $k$ -mesh of  $10 \times 10 \times 1$  and a cutoff energy of 600 Ry. The criterion of energy convergence OpenMX is set to  $1.0 \times 10^{-6}$  Hartree/Bohr. The structures used in OpenMX were relaxed by VASP and were not reoptimized in OpenMX calculations. The discontinuous transition feature of interlayer coupling and magnetic moment of the Fe5 atom was still observed in OpenMX.

### 3. RESULTS AND ANALYSIS

**3.1. Interlayer Magnetic Coupling Spike Induced by In-Plane Strain.** The crystal structure and magnetic models of FSGT are depicted in Figure 1a. Our model uses data collected

on quenched crystals with the space group  $R3m$  (No. 160).<sup>31</sup> The F5GT bulk material is formed by the staggered stacking of three monolayers of F5GT. We constructed a  $2 \times 1 \times 1$  supercell (six layers) to model the interlayer FM and AFM structures. To our surprise, the evolution of ILMC (Figure 1b) with in-plane biaxial strain exhibits an increase by an order, from 1.15 to 12.79 meV/f.u. at a 3% in-plane biaxial strain. As the strain further increases, the ILMC drops down rapidly, forming an ILMC spike at a 3% in-plane tensile strain. This discontinuous transition feature in ILMC is preserved in the uniaxial strain (Figure S1a), but the critical strain value shifted from 3% in the biaxial strain to 4% in the uniaxial strain. Furthermore, we also observed a sign-reverse of the ILMC at an 8% in-plane biaxial strain, indicating that the ILMC changes from the antiferromagnetic (AFM) to the ferromagnetic (FM) state. As for the off-plane strain, the ILMC evolves much more gently than that of the in-plane strain. The ILMC reaches the maximum of 2.3 meV/f.u. at a 2% off-plane strain and hits the minimum of  $-0.1$  meV/f.u. at a  $-8\%$  off-plane compressive strain (Figure S1b). Therefore, the ILMC could also be tuned from the AFM to the FM state by applying a  $-8\%$  off-plane compressive strain. Figure S1c presents the ILCC evolution with in-plane and off-plane strains. An ILCC jump (red line) could also be observed when an in-plane biaxial strain is applied, in line with the observation of Figure 1b. Conclusively, we find an unusual ILMC spike and tunable ILMC properties in F5GT. These properties may hold a promising prospect for designing novel spintronic devices.

**3.2. Mechanism of ILMC and Magnetic Moment of the Fe5 Ion.** To elucidate the ILMC spikes induced by the in-plane strain, we present the evolution of the magnetic moment of Fe ions under various strains. As plotted in Figure 2a, the magnetic moments of Fe1–Fe4 ions increase monotonically with strain. However, the magnetic moments of Fe5 ions undergo a drastic jump from  $-0.1$  to  $1.4 \mu_B$  at about 3% tensile strain, highly consistent with the change of ILMC. Moreover, the obvious spin-polarization of the Fe5 ion can be observed at a 3% biaxial strain (Figure 2b, inset). The rapid decline of ILMC may be related to the noticeable increase ( $0.13e$ ) in the Bader charge of Fe5 ions within the 3–4% in-plane strain range, which rearranges the charge density distribution remarkably. The charge change of the Fe5 atom is mainly attributed to the nearby Te1 atom, which shows an obvious decrease in that strain range (Figure S2). Regarding the off-plane strain (Figure S3), there is no significant enhancement observed in the magnetic moments of the five Fe ions, as their evolution appears to be smooth. Therefore, we mainly focus on the in-plane strain.

The evolutions of bond lengths and angles around Fe5 ions with the in-/off-plane strain are illustrated in Figure S4. The variation of the Fe5–Ge bond length shows a distinct change within the 2–4% in-plane strain range (Figure S4a, highlighted by red dashed circles), indicating the drastic structure change induced by the magnetic evolution. However, the bond angles around the Fe5 ion exhibit a smooth and monotonous variation, with only a small perturbation in the angle  $\angle\text{Te1-Fe5-Ge}$  observed within the 2–4% in-plane strain range (Figure S4b). Therefore, we conclude that the increased magnetic moment of Fe5 mainly affects the bond distance rather than bond angles. As for the off-plane strain, there is no significant structural variation observed, as both bond lengths and bond angles exhibit a smooth and monotonous evolution (Figure S4c,d).

In Figure 2c,d, we present the partial density of states (PDOS) before and after the magnetic moment increase of the Fe5 ion. Since F5GT belongs to the hexagonal crystal system, the Fe ion belongs to the  $D_{3h}$  symmetry. Its orbitals split into three states, namely,  $A'_1(d_z^2)$ ,  $E'(d_{x^2-y^2}/d_{xy})$ , and  $E''(d_{yz}/d_{xz})$ . As shown in Figure 2c,d, the  $A'_1$  state is fully occupied at 2 and 3% in-plane biaxial strains. Both  $E'$  and  $E''$  states are partially occupied and distribute evenly at a 2% in-plane biaxial strain, leading to a low-spin configuration. As for a 3% in-plane strain,  $E'$  and  $E''$  states show an apparent polarization, resulting in the high-spin configuration.

Decomposed Mulliken population analysis<sup>38,39</sup> is presented in Figure 3. Although Figure 3a,b shows that  $A'_1(d_z^2)$  is the dominant contribution in both the spin-up and -down channels, the difference in its values between these two channels is relatively smaller than that of  $E'(d_{x^2-y^2}/d_{xy})$  and  $E''(d_{yz}/d_{xz})$  (Figure 3d). Thus, the  $E'(d_{x^2-y^2}/d_{xy})$  and  $E''(d_{yz}/d_{xz})$  states are the major contributors to the magnetic moment of Fe5. Meanwhile, the sharp increase/decrease of all spin-up/-down channel orbitals within the 2–3% strain range (Figure 3a,b) indicates the presence of spin splitting in the Fe5 ion. This result is supported by the energy band diagram (Figure S5b,c), where the spin-up/-down component moves down/up around the Fermi level with the strain.

Figure 3c shows the summed-up value of the spin-up and spin-down channels. The sum of  $E'(d_{x^2-y^2}/d_{xy})$  orbitals presents a distinct increase at 2–3% strains, whereas the  $E''(d_{yz}/d_{xz})$  orbitals exhibit a decrease. It implies that the transfer of charge from  $E''(d_{yz}/d_{xz})$  orbitals to  $E'(d_{x^2-y^2}/d_{xy})$  orbitals is a crucial factor contributing to the ILMC spike. This result can also be confirmed by occupied bands (Figure S5a) and band diagrams (Figure S5b,c). The number of occupied bands in the spin-up channel increases from 39 to 40 at a 2% in-plane strain (Figure S5a), in agreement with the ILMC spike. With a 3% in-plane strain applied, the blue-dashed band in the spin-up channel shifts downward and intersects the Fermi level within the  $Y_2 \sim \Gamma$   $k$ -point region. The band in the aforementioned  $k$ -point region is primarily composed of the  $E'(d_{x^2-y^2}/d_{xy})$  orbitals (Figure S6). This finding aligns well with the Mulliken population analysis. All in all, we propose that the increase in the magnetic moment of the Fe5 ion is the driving force behind the observed ILMC. The significant change in the magnetic moment is a result of two processes as plotted in Figure 3e, i.e., the charge transfer from the  $E''(d_{yz}/d_{xz})$  orbital to the  $E'(d_{x^2-y^2}/d_{xy})$  orbital and the spin splitting of spin-up/-spin-down channels.

**3.3. Evolution of Intralayer Exchange Parameters and Magnetic Anisotropy Energy.** The exchange parameters are of significance in determining the magnetic properties and Curie temperature of the single-layer system.<sup>40,41</sup> As plotted in Figure 4, each Fe5 ion has its first, second, and third nearest neighbor Fe ions, corresponding to the first ( $J_1$ ), second ( $J_2$ ), and third ( $J_3$ ) intralayer Heisenberg exchange parameters. The distances from each Fe5 to its three neighbors are 2.4, 2.8, and 3.7 Å, respectively. The calculated  $J_1$ ,  $J_2$ , and  $J_3$  parameters with in-plane strain are presented in Figure 4. The exchange interaction around the Fe5 ion experiences a dramatic change within the in-plane strain range of 2–3%. Specifically, the dominant contribution ( $J_1$ ) soars to 13.0 (3%) from 3.2 (2%) meV.  $J_2$  also presents a sharp increase from negative ( $-1.3$  meV) to positive (6.1 meV). Conversely,  $J_3$  displays an opposite trend, declining from a positive value of 1.0 meV to a negative value of  $-3.5$  meV. The summed-up value of  $J_1$ ,  $J_2$ ,

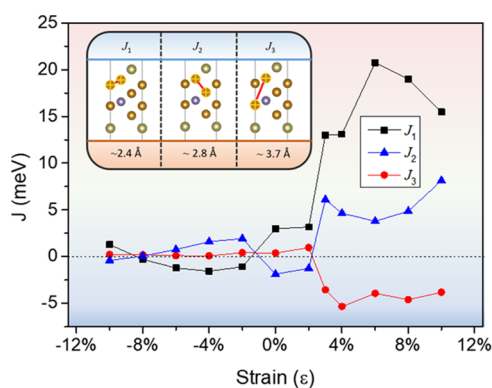


**Figure 4.** Evolution of the first ( $J_1$ ), second ( $J_2$ ), and third ( $J_3$ ) nearest neighbor Heisenberg exchange parameters around the Fe5 ion.

and  $J_3$  demonstrates a noticeable improvement within 2–3% extensile strain range, suggesting a substantial enhancement of intralayer magnetic coupling.

The magnetic anisotropy energy (MAE), one of the most important properties of 2D magnetic materials, is sensitive to strain and film thickness.<sup>42</sup> Here, we have chosen the AB stack model randomly for studies, as different stack models show consistent evolving trends in both ILCC and ILMC (Figure S7a,b). The evolution of MAE in F5GT with various thicknesses and in-plane strains is presented in Figure 5. The acute increase in the magnetic moment of the Fe5 ion has resulted in a corresponding sharp increase in MAE in the single-layer, double-layer, and bulk systems. Regarding the strain-tunable magnetic anisotropy, F5GT displays a preference for an in-plane magnetic configuration in the absence of

strain. However, two distinct switching points between in-plane and off-plane magnetic configurations can be observed in single-layer F5GT at around –6 and 8% biaxial strains (Figure 5a). After the introduction of interlayer coupling, the magnetic moment of the Fe ion varies from 0.1 to  $-0.3 \mu_B$ , resulting in a slight delay of the magnetic tipping point (Figure S7c,d). As for MAE, the inclusion of interlayer interaction shifts the switching point, previously observed at around an 8% biaxial strain in the single layer, backward to the 2–3% strain range (Figure 5b,c). The MAE differences (between 2 and 3% in-plane strains) are strongly enhanced from 0.47 to 0.85 meV/f.u. with thicknesses. Compared to the double layers, the bulk system exhibits stronger interlayer coupling, leading to a notably enhanced stability of the off-plane configuration. This is supported by the almost doubled value of its MAE at a 3% in-plane strain. In conclusion, the interlayer coupling in the F5GT system significantly enhances its MAE, leading to a switch between in-plane and off-plane configurations within the 2–3% in-plane strain range.

#### 4. CONCLUSIONS

In conclusion, our theoretical investigation of the evolution of interlayer coupling in F5GT with strains has revealed a remarkable spike in the ILMC. Within the 2–3% in-plane biaxial strain range, the ILMC increases rapidly from 1.15 to 12.79 meV/f.u. The acute enhancement in the magnetic moment of the Fe5 ion, from  $-0.1 \mu_B$  to  $1.4 \mu_B$  at a 3% in-plane biaxial strain, coincides well with the ILMC spike. Moreover, the electronic structure analysis reveals that the mechanism involves charge transfer from  $E'$  ( $d_{x^2-y^2}/d_{xy}$ ) to  $E''$  ( $d_{yz}/d_{xz}$ ) and spin splitting of the Fe5 ion. Additionally, the

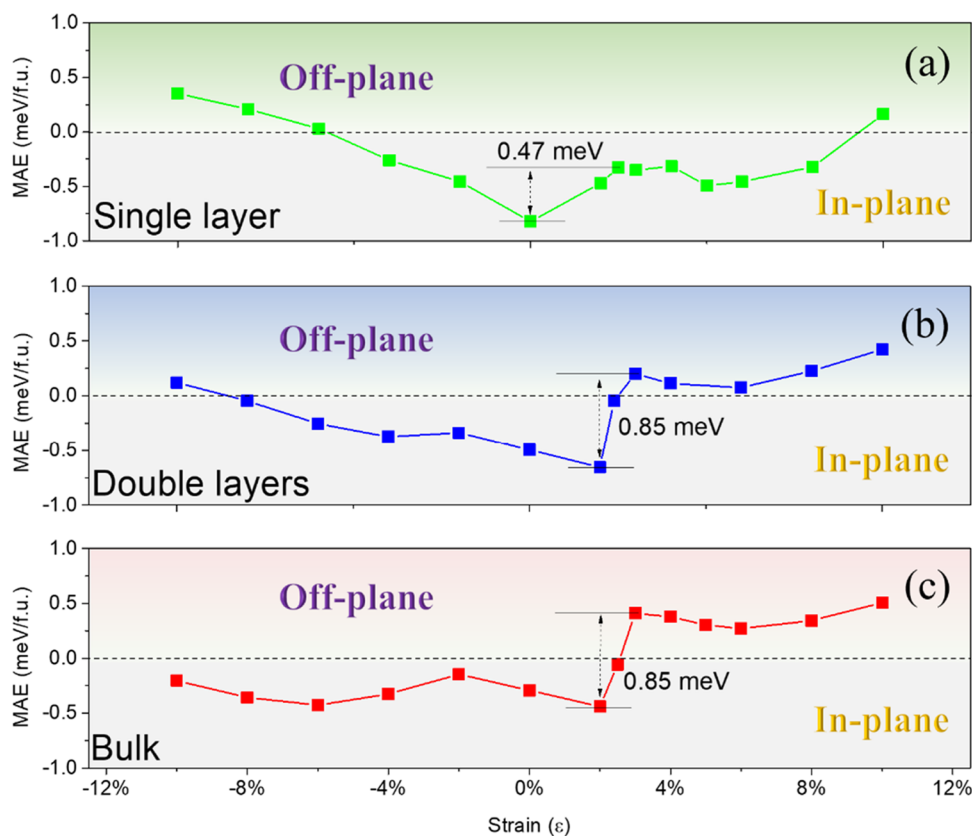


**Figure 5.** Calculated magnetic anisotropy energy (MAE) of the (a) single layer, (b) double layers, and (c) bulk models.

applied 3% in-plane strain may also result in a noticeable enhancement of the intralayer magnetic coupling. Incorporating interlayer coupling into the system can markedly increase its MAE, which triggers the transition of the in-plane and off-plane configurations within a strain range of 2–3%. With these distinctive characteristics, FSGT is promising for future spintronic applications and designs.

## ■ ASSOCIATED CONTENT

### Data Availability Statement

All data needed to evaluate the conclusions in the paper are present in the paper and/or the Supplementary Materials. Additional data related to this paper may be requested from the authors.

### SI Supporting Information

The Supporting Information is available free of charge at <https://pubs.acs.org/doi/10.1021/acs.jpcc.3c03788>.

ILMC and ILCC evolution with different types of strains; Bader charge variation; magnetic moment variation with off-plane strains; variation of bond lengths and angles; band structure diagrams; projected band structures of the FeS atom; and ILMC evolution with different models (PDF)

## ■ AUTHOR INFORMATION

### Corresponding Authors

**Yu-Jun Zhao** – Department of Physics, South China University of Technology, Guangzhou 510640, China; [orcid.org/0000-0002-6923-1099](https://orcid.org/0000-0002-6923-1099); Email: [zhaoyj@scut.edu.cn](mailto:zhaoyj@scut.edu.cn)

**Wen-Tong Geng** – School of Materials Science and Engineering, Hainan University, Haikou 570228, China; [orcid.org/0000-0002-9838-5644](https://orcid.org/0000-0002-9838-5644); Email: [geng@hainanu.edu.cn](mailto:geng@hainanu.edu.cn)

### Authors

**Wen-Qiang Xie** – School of Materials Science and Engineering, Hainan University, Haikou 570228, China; Department of Physics, South China University of Technology, Guangzhou 510640, China; [orcid.org/0009-0009-1211-3495](https://orcid.org/0009-0009-1211-3495)

**Chang-Chun He** – Department of Physics, South China University of Technology, Guangzhou 510640, China

**Xiao-Bao Yang** – Department of Physics, South China University of Technology, Guangzhou 510640, China; [orcid.org/0000-0001-8851-1988](https://orcid.org/0000-0001-8851-1988)

Complete contact information is available at: <https://pubs.acs.org/doi/10.1021/acs.jpcc.3c03788>

### Notes

The authors declare no competing financial interest.

## ■ ACKNOWLEDGMENTS

This work was supported by the NSFC (Grant No. 12074126), the Foundation for Innovative Research Groups of the National Natural Science Foundation of China (Grant No. 51621001), and the Natural Science Foundation of Guangdong Province of China (Grant No. 2016A030312011). The computer times at the National Supercomputing Center in Guangzhou (NSCCGZ) are gratefully acknowledged.

## ■ REFERENCES

- (1) Wang, Q. H.; Bedoya-Pinto, A.; Blei, M.; Dismukes, A. H.; Hamo, A.; Jenkins, S.; Koperski, M.; Liu, Y.; Sun, Q.-C.; Telford, E. J.; et al. The magnetic genome of two-dimensional van der Waals materials. *ACS Nano* **2022**, *16*, 6960–7079.
- (2) Burch, K. S.; Mandrus, D.; Park, J.-G. Magnetism in two-dimensional van der Waals materials. *Nature* **2018**, *563*, 47–52.
- (3) Li, D.; Frauenheim, T.; He, J. Robust giant magnetoresistance in 2D van der Waals molecular magnetic tunnel junctions. *ACS Appl. Mater. Interfaces* **2021**, *13*, 36098–36105.
- (4) Li, X.; Su, Y.; Zhu, M.; Zheng, F.; Zhang, P.; Zhang, J.; Lü, J.-T. Current-perpendicular-to-plane giant magnetoresistance effect in van der Waals heterostructures. *Phys. Rev. Appl.* **2021**, *16*, No. 034052.
- (5) Yang, W.; Cao, Y.; Han, J.; Lin, X.; Wang, X.; Wei, G.; Lv, C.; Bournel, A.; Zhao, W. Spin-filter induced large magnetoresistance in 2D van der Waals magnetic tunnel junctions. *Nanoscale* **2021**, *13*, 862–868.
- (6) Zhu, W.; Song, C.; Han, L.; Guo, T.; Bai, H.; Pan, F. Van der Waals lattice-induced colossal magnetoresistance in Cr<sub>2</sub>Ge<sub>2</sub>Te<sub>6</sub> thin flakes. *Nat. Commun.* **2022**, *13*, No. 6428.
- (7) Ribeiro, M.; Gentile, G.; Marty, A.; Dosenovic, D.; Okuno, H.; Vergnaud, C.; Jacquot, J.-F.; Jalabert, D.; Longo, D.; Ohresser, P.; et al. Large-scale epitaxy of two-dimensional van der Waals room-temperature ferromagnet Fe<sub>3</sub>GeTe<sub>2</sub>. *npj 2D Mater. Appl.* **2022**, *6*, No. 10.
- (8) Tan, C.; Xie, W.-Q.; Zheng, G.; Aloufi, N.; Albarakati, S.; Algarni, M.; Li, J.; Partridge, J.; Culcer, D.; Wang, X.; et al. Gate-controlled magnetic phase transition in a van der Waals magnet Fe<sub>3</sub>GeTe<sub>2</sub>. *Nano Lett.* **2021**, *21*, 5599–5605.
- (9) Albarakati, S.; Xie, W.-Q.; Tan, C.; Zheng, G.; Algarni, M.; Li, J.; Partridge, J.; Spencer, M. J.; Farrar, L.; Xiong, Y.; et al. Electric Control of Exchange Bias Effect in FePS<sub>3</sub>–Fe<sub>3</sub>GeTe<sub>2</sub> van der Waals Heterostructures. *Nano Lett.* **2022**, *22*, 6166–6172.
- (10) Dai, Z.; Liu, L.; Zhang, Z. Strain engineering of 2D materials: issues and opportunities at the interface. *Adv. Mater.* **2019**, *31*, No. 1805417.
- (11) Du, J.; Yu, H.; Liu, B.; Hong, M.; Liao, Q.; Zhang, Z.; Zhang, Y. Strain engineering in 2D material-based flexible optoelectronics. *Small Methods* **2021**, *5*, No. 2000919.
- (12) Han, Y.; Gao, L.; Zhou, J.; Hou, Y.; Jia, Y.; Cao, K.; Duan, K.; Lu, Y. Deep elastic strain engineering of 2D materials and their twisted bilayers. *ACS Appl. Mater. Interfaces* **2022**, *14*, 8655–8663.
- (13) Sun, Y.; Liu, K. Strain engineering in functional 2-dimensional materials. *J. Appl. Phys.* **2019**, *125*, No. 082402.
- (14) Hu, X.; Zhao, Y.; Shen, X.; Krashennnikov, A. V.; Chen, Z.; Sun, L. Enhanced ferromagnetism and tunable magnetism in Fe<sub>3</sub>GeTe<sub>2</sub> monolayer by strain engineering. *ACS Appl. Mater. Interfaces* **2020**, *12*, 26367–26373.
- (15) Qi, Y.; Sadi, M. A.; Hu, D.; Zheng, M.; Wu, Z.; Jiang, Y.; Chen, Y. P. Recent progress in strain engineering on van der Waals 2D materials: Tunable electrical, electrochemical, magnetic and optical properties. *Adv. Mater.* **2022**, *35*, No. 2205714.
- (16) Wang, K.; Hu, T.; Jia, F.; Zhao, G.; Liu, Y.; Solovyev, I. V.; Pyatakov, A. P.; Zvezdin, A. K.; Ren, W. Magnetic and electronic properties of Cr<sub>2</sub>Ge<sub>2</sub>Te<sub>6</sub> monolayer by strain and electric-field engineering. *Appl. Phys. Lett.* **2019**, *114*, No. 092405.
- (17) Wang, M.-C.; Huang, C.-C.; Cheung, C.-H.; Chen, C.-Y.; Tan, S. G.; Huang, T.-W.; Zhao, Y.; Zhao, Y.; Wu, G.; Feng, Y.-P.; et al. Prospects and opportunities of 2D van der Waals magnetic systems. *Ann. Phys.* **2020**, *532*, No. 1900452.
- (18) Joe, M.; Yang, U.; Lee, C. First-principles study of ferromagnetic metal Fe<sub>3</sub>GeTe<sub>2</sub>. *Nano Mater. Sci.* **2019**, *1*, 299–303.
- (19) Gonzalez, J. M.; Oleynik, I. I. Layer-dependent properties of SnS<sub>2</sub> and SnSe<sub>2</sub> two-dimensional materials. *Phys. Rev. B* **2016**, *94*, No. 125443.
- (20) Li, L.; Kim, J.; Jin, C.; Ye, G. J.; Qiu, D. Y.; da Jornada, F. H.; Shi, Z.; Chen, L.; Zhang, Z.; Yang, F.; et al. Direct observation of the layer-dependent electronic structure in phosphorene. *Nat. Nanotechnol.* **2017**, *12*, 21–25.

- (21) Zheng, G.; Xie, W.-Q.; Albarakati, S.; Algarni, M.; Tan, C.; Wang, Y.; Peng, J.; Partridge, J.; Farrar, L.; Yi, J.; et al. Gate-tuned interlayer coupling in van der Waals ferromagnet Fe<sub>3</sub>GeTe<sub>2</sub> nanoflakes. *Phys. Rev. Lett.* **2020**, *125*, No. 047202.
- (22) Song, T.; Cai, X.; Tu, M. W.-Y.; Zhang, X.; Huang, B.; Wilson, N. P.; Seyler, K. L.; Zhu, L.; Taniguchi, T.; Watanabe, K.; et al. Giant tunneling magnetoresistance in spin-filter van der Waals heterostructures. *Science* **2018**, *360*, 1214–1218.
- (23) Jiang, S.; Shan, J.; Mak, K. F. Electric-field switching of two-dimensional van der Waals magnets. *Nat. Mater.* **2018**, *17*, 406–410.
- (24) León, A. M.; González, J. W.; Mejía-López, J.; de Lima, F. C.; Morell, E. S. Strain-induced phase transition in CrI<sub>3</sub> bilayers. *2D Mater.* **2020**, *7*, No. 035008.
- (25) Huang, X.; Xu, J.; Zeng, R.; Jiang, Q.; Nie, X.; Chen, C.; Jiang, X.; Liu, J.-M. Li-ion intercalation enhanced ferromagnetism in van der Waals Fe<sub>3</sub>GeTe<sub>2</sub> bilayer. *Appl. Phys. Lett.* **2021**, *119*, No. 012405.
- (26) Hohenberg, P.; Kohn, W. Inhomogeneous electron gas. *Phys. Rev.* **1964**, *136*, B864–B871.
- (27) Kohn, W.; Sham, L. J. Self-consistent equations including exchange and correlation effects. *Phys. Rev.* **1965**, *140*, A1133–A1138.
- (28) Hafner, J. *Ab-initio* simulations of materials using VASP: Density-functional theory and beyond. *J. Comput. Chem.* **2008**, *29*, 2044–2078.
- (29) Blöchl, P. E. Projector augmented-wave method. *Phys. Rev. B* **1994**, *50*, 17953–17979.
- (30) Perdew, J. P.; Burke, K.; Ernzerhof, M. Generalized gradient approximation made simple. *Phys. Rev. Lett.* **1996**, *77*, 3865–3868.
- (31) Stahl, J.; Shlaen, E.; Johrendt, D. The van der Waals ferromagnets Fe<sub>5-δ</sub>GeTe<sub>2</sub> and Fe<sub>5-δ-x</sub>NixGeTe<sub>2</sub> – crystal structure, stacking faults, and magnetic properties. *Z. Anorg. Allg. Chem.* **2018**, *644*, 1923–1929.
- (32) Jang, S. W.; Yoon, H.; Jeong, M. Y.; Ryee, S.; Kim, H.-S.; Han, M. J. Origin of ferromagnetism and the effect of doping on Fe<sub>3</sub>GeTe<sub>2</sub>. *Nanoscale* **2020**, *12*, 13501–13506.
- (33) Monkhorst, H. J.; Pack, J. D. Special points for Brillouin-zone integrations. *Phys. Rev. B* **1976**, *13*, 5188.
- (34) Grimme, S.; Antony, J.; Ehrlich, S.; Krieg, H. A consistent and accurate *ab initio* parametrization of density functional dispersion correction (DFT-D) for the 94 elements H-Pu. *J. Chem. Phys.* **2010**, *132*, No. 154104.
- (35) He, X.; Helbig, N.; Verstraete, M. J.; Bousquet, E. TB2J: A python package for computing magnetic interaction parameters. *Comput. Phys. Commun.* **2021**, *264*, No. 107938.
- (36) Boker, S.; Neale, M.; Maes, H.; Wilde, M.; Spiegel, M.; Brick, T.; Spies, J.; Estabrook, R.; Kenny, S.; Bates, T.; et al. OpenMX: an open source extended structural equation modeling framework. *Psychometrika* **2011**, *76*, 306–317.
- (37) Liechtenstein, A. I.; Katsnelson, M. I.; Antropov, V. P.; Gubanov, V. A. Local spin density functional approach to the theory of exchange interactions in ferromagnetic metals and alloys. *J. Magn. Mater.* **1987**, *67*, 65–74.
- (38) Mulliken, R. S. Electronic population analysis on LCAO–MO molecular wave functions. II. Overlap populations, bond orders, and covalent bond energies. *J. Chem. Phys.* **1955**, *23*, 1841–1846.
- (39) Carbó-Dorca, R.; Bultinck, P. Quantum mechanical basis for Mulliken population analysis. *J. Math. Chem.* **2004**, *36*, 231–239.
- (40) Kan, M.; Adhikari, S.; Sun, Q. Ferromagnetism in MnX<sub>2</sub> (X = S, Se) monolayers. *Phys. Chem. Chem. Phys.* **2014**, *16*, 4990–4994.
- (41) Xie, W.-Q.; Lu, Z.-W.; He, C.-C.; Yang, X.-B.; Zhao, Y.-J. Theoretical study of tunable magnetism of two-dimensional MnSe<sub>2</sub> through strain, charge, and defect. *J. Phys.: Condens. Matter* **2021**, *33*, No. 215803.
- (42) Webster, L.; Yan, J.-A. Strain-tunable magnetic anisotropy in monolayer CrCl<sub>3</sub>, CrBr<sub>3</sub>, and CrI<sub>3</sub>. *Phys. Rev. B* **2018**, *98*, No. 144411.